ELASTIC WAVE DIFFRACTION OF A PISTON SOURCE AND ITS EFFECT ON ATTENUATION MEASUREMENT

by

X.M. Tang, M.N. Toksöz, and C.H. Cheng

Earth Resources Laboratory
Department of Earth, Atmospheric, and Planetary Sciences
Massachusetts Institute of Technology
Cambridge, MA 02139

ABSTRACT

The radiation of an elastic wave field from a plane piston source is formulated using the representation theorem, in which the Green's function for an elastic half space is employed. On the basis of this formulation, we derive the radiated elastic wave field for both compressional and shear wave sources. We study the diffraction of elastic waves incident on a receiver that is coaxially aligned with the source. We present a procedure in which both numerical and asymptotic techniques are employed to allow us to evaluate the diffraction effects in any frequency range of interest. We compare the elastic diffraction with the acoustic diffraction and find that they are different in the near field of the piston source due to the coupling between shear and compressional components in the elastic case. In the far field, however, the elastic diffraction approaches the acoustic diffraction. With the help of ultrasonic laboratory measurements, we test the theoretical results and find that the theory and experiments agree well. An important result of this study is that in attenuation measurements with pulse propagation techniques where spectral ratio relative to a standard sample or ratio of samples of the same material but of different lengths is used, it is necessary to correct for diffraction effects. In the attenuation measurement using spectral ratio of a sample and a standard reference sample, the attenuation can be overestimated, while in the attenuation measurement using a spectral ratio of samples of different lengths, the attenuation can be significantly underestimated, if corrections for diffraction effects are not made.

INTRODUCTION

A cylindrical (or piston) shaped transducer is an important signal generating device in many scientific applications. A common characteristic of all piston sources is the

diffraction effects in the radiated wave field. For the acoustic wave field, this phenomenon has been well studied by many authors (Williams, 1951; Bass, 1958; Gitis and Khimunin, 1969; Harris, 1981; Tang et al., 1988). By comparison, the nature of the elastic wave field radiated by a planar piston has not been studied in detail. In practice, however, many important applications, such as rock physics and nondestructive testing of solids, require the solution of the elastic problem. Needless to say, the treatment of the elastic case is much more complicated than that of the acoustic case. In addition to the vector nature of the elastic field, one needs to consider the vector nature of the source vibrations, because a piston source can be made to generate either shear or compressional waves, or both. Moreover, as in the acoustic case, one also needs to consider the arbitrarily shaped piston sources. As will be shown in the next section, all these problems can be formulated into a compact form and solved using the elastic representation theorem.

In the first part of this paper, we formulate the problem of elastic radiation by an arbitrarily shaped surface stress source and calculate the radiated wave fields for both shear and compressional circular piston sources and their average fields incident on a receiver that is coaxially aligned with the source. In the second part, we present a procedure using both numerical and asymptotic methods and evaluate the diffraction effects in the average wave field. In the third part, we give the results of the evaluations and compare the elastic radiation with the acoustic radiation. In the final part, by conducting a laboratory experiment, we compare our theory with experimental results and analyze the effects of diffraction on the elastic attenuation measurements.

FORMULATION OF THE ELASTIC RADIATION OF A PISTON SOURCE

The present problem can be formulated as the radiation of a surface distribution of stress vibrations into an elastic half space. The frequency domain elastic wave equation of motion for isotropic homogeneous media may be written as

$$(\lambda + 2\mu) \bigtriangledown (\bigtriangledown \cdot \vec{u}) - \mu \bigtriangledown \times (\bigtriangledown \times \vec{u}) + \rho\omega^2 \vec{u} = 0, \tag{1}$$

where $\vec{u} = (u_1, u_2, u_3)$ is the displacement field, λ and μ are Lamé constants, ω is the angular frequency, and ρ is the density of the medium. The solution of Eq. (1) for a medium free of body forces is given by the representation theorem (Aki and Richards, 1980), which, in terms of tensor notations, can be expressed as

$$u_j = \int\int_S G_{jl}\sigma_{lk} n_k dS - \int\int_S u_p c_{pklq} \frac{\partial G_{jl}}{\partial x'_q} n_k dS, \tag{2}$$

where $G_{jl}(x_1, x_2, x_3, \omega; x'_1, x'_2, x'_3)$ is the tensor Green's function, x_j and x'_j $(j = 1, 2, 3)$ refer to the field and source points, respectively, c_{pklq} is the elastic tensor, σ_{lk} is the

given stress distribution on the surface S, and n_k is the normal to this surface. In this formulation, the summation convention is assumed and the integration is over the source point (x_1', x_2', x_3'). If we solve the boundary value problem by finding the tensor Green's function such that its generated traction $c_{pklq} n_k \frac{\partial G_{jl}}{\partial x_q'}$ vanishes on S, then the problem can be reduced to the evaluation of only the first integral in Eq. (2). For the elastic half space where S is now the $x_3' = 0$ plane, Johnson (1974) obtained the Green's function for a source point located at $(0, 0, x_3')$. It is easy to generalize his Green's function for any source point (x_1', x_2', x_3') in the half space and show that such a Green's function is given by the following two-dimensional inverse Fourier transform:

$$G_{jl}(x_1, x_2, x_3, \omega; x_1', x_2', x_3') = \frac{1}{4\pi^2} \int_{-\infty}^{\infty} \int_{-\infty}^{\infty} \widetilde{G}_{jl}(k_1, k_2, x_3, \omega; 0, 0, x_3') e^{i[k_1(x_1 - x_1') + k_2(x_2 - x_2')]} dk_1 dk_2, \tag{3}$$

where k_1, k_2 are the dummy wavenumber variables and $\widetilde{G}_{lj}(k_1, k_2, x_3, \omega; 0, 0, x_3')$ in the integrand has been obtained by Johnson (1974, Eqs. 9 and 10). To perform the integration in the first integral in Eq. (2), we set $x_3' = 0$ in Eq. (3) and derive from Johnson's Eqs. (9) and (10) the matrix expression for the two-dimensional Fourier transform of the tensor Green's function evaluated at $x_1' = x_2' = x_3' = 0$:

$$\begin{aligned} &\widetilde{\mathbf{G}}(k_1, k_2, x_3, \omega; 0, 0, 0) \\ &= \frac{e^{-\nu x_3}}{\mu F(k)} \begin{pmatrix} -2k_1^2\nu' & -2k_1k_2\nu' & ik_1h \\ -2k_1k_2\nu' & -2k_2^2\nu' & ik_2h \\ 2ik_1\nu\nu' & 2ik_2\nu\nu' & \nu h \end{pmatrix} - \frac{e^{-\nu' x_3}}{\nu' \mu F(k)} \\ &\times \begin{pmatrix} k_2^2(4\nu\nu' - h) - \nu'^2 h & k_1k_2(h - 4\nu\nu') & 2ik_1\nu\nu'^2 \\ k_1k_2(h - 4\nu\nu') & k_1^2(4\nu\nu' - h) - \nu'^2 h & 2ik_2\nu\nu'^2 \\ ik_1\nu' h & ik_2\nu' h & 2\nu\nu' k^2 \end{pmatrix}, \end{aligned} \tag{4}$$

where

$$\begin{aligned} &k_\alpha = \omega/\alpha, && k_\beta = \omega/\beta, \\ &k = \sqrt{k_1^2 + k_2^2}, && h = 2k^2 - k_\beta^2, \\ &\nu = \sqrt{k^2 - k_\alpha^2}, && \nu' = \sqrt{k^2 - k_\beta^2}, \\ &F(k) = h^2 - 4\nu\nu' k^2, \end{aligned}$$

and α and β are compressional and shear velocities, respectively. Once the Green's function is known, the radiated elastic displacement can be calculated using

$$\begin{aligned} u_j(x_1, x_2, x_3, \omega) &= \frac{1}{4\pi^2} \int_{-\infty}^{\infty} \int_{-\infty}^{\infty} \widetilde{G}_{jl}(k_1, k_2, x_3, \omega; 0, 0, 0) e^{i(k_1 x_1 + k_2 x_2)} \\ &\times \left[\int \int_S \sigma_{l3}(x_1', x_2', \omega) e^{-i(k_1 x_1' + k_2 x_2')} dx_1' dx_2' \right] dk_1 dk_2, \end{aligned} \tag{5}$$

where we have used $n_k = \delta_{k3}$ (δ_{ij} is the Kronecker delta) for the normal of S. Eq. (5), together with the Fourier transform of the Green's function given by Eq. (4), gives

the radiated elastic wave field for any given stress distribution σ_{l3} over the area S on the $x_3' = 0$ plane. In general, the surface integral (in square bracket) in Eq. (5) is equivalent to the two-dimensional Fourier transform of the surface stress distribution.

In practical applications, there are two types of piston sources. One is the compressional source whose vibrations are normal to the surface, the other is the shear source whose vibrations are parallel to the piston surface. We let this latter polarization be in x_1 direction. In most cases, the piston sources are circular. We now proceed to find the radiated fields of circular compressional and shear sources. We assume a constant stress distribution over a circular source of radius a. Thus the surface integral can be written and integrated out as

$$\int_{-\infty}^{\infty}\int_{-\infty}^{\infty}\sigma_{l3}(\omega)H\left(a-\sqrt{x_1'^2+x_2'^2}\right)e^{-i(k_1x_1'+k_2x_2')}dx_1'dx_2' = \sigma_{l3}(\omega)\frac{a}{k}J_1(ka) \qquad (6)$$

where H represents the step function, $J_1(ka)$ is the Bessel function, and $\sigma_{l3}(\omega)$ is the source stress spectrum; $l = 3$ means that the stresses are normal to the $x_3' = 0$ plane (compressional source), and $l = 1$ means that the stresses are in the x_1' direction acting on the $x_3' = 0$ plane (shear source). The above integration is performed by making the following transformations

$$\begin{array}{ll} k_1 = kcos\theta & k_2 = ksin\theta \\ x_1' = r'cos\phi & x_2' = r'sin\phi \end{array} \qquad (7)$$

Using the same transformations, but replacing x_1', x_2', and r' with x_1, x_2, and r, we can now simplify the integration over k_1 and k_2 in Eq. (5). We also use the following identities

$$\begin{aligned}
\int_0^{2\pi} e^{ikrcos(\theta-\phi)}sin\theta cos\theta d\theta &= -\pi J_2(kr)sin2\phi \\
\int_0^{2\pi} e^{ikrcos(\theta-\phi)}d\theta &= 2\pi J_0(kr) \\
\int_0^{2\pi} e^{ikrcos(\theta-\phi)}sin^2\theta d\theta &= \pi J_0(kr) + \pi J_2(kr)cos2\phi \\
\int_0^{2\pi} e^{ikrcos(\theta-\phi)}sin\theta d\theta &= 2\pi i J_1(kr)sin\phi \\
\int_0^{2\pi} e^{ikrcos(\theta-\phi)}cos^2\theta d\theta &= \pi J_0(kr) - \pi J_2(kr)cos2\phi \\
\int_0^{2\pi} e^{ikrcos(\theta-\phi)}cos\theta d\theta &= 2\pi i J_1(kr)cos\phi, \qquad (8)
\end{aligned}$$

where J_0, J_1, and J_2 are Bessel functions of the first kind and order zero, one, and two, respectively. With the use of the transformations and identities, the two-dimensional integration in Eq. (5) is reduced to one-dimensional integration which significantly facilitates its numerical evaluations. Replacing x_3 by z to comply with convention, we

now express the radiated displacement fields $u_j(r,\phi,z,\omega)$ for the compressional and shear sources as follows:
The compressional source [$l = 3$ in Eq. (5)]:

$$\begin{aligned}
u_1 &= \frac{a\sigma_{33}(\omega)cos\phi}{2\pi\mu}\int_0^\infty \left[\frac{2k^2-k_\beta^2}{F(k)}e^{-\nu z} - \frac{2\nu\nu'}{F(k)}e^{-\nu' z}\right] J_1(ka)J_1(kr)kdk \\
u_2 &= \frac{a\sigma_{33}(\omega)sin\phi}{2\pi\mu}\int_0^\infty \left[\frac{2k^2-k_\beta^2}{F(k)}e^{-\nu z} - \frac{2\nu\nu'}{F(k)}e^{-\nu' z}\right] J_1(ka)J_1(kr)kdk \\
u_3 &= -\frac{a\sigma_{33}(\omega)}{2\pi\mu}\int_0^\infty \left[\frac{2k^2-k_\beta^2}{F(k)}\nu e^{-\nu z} - \frac{2k^2\nu}{F(k)}e^{-\nu' z}\right] J_1(ka)J_0(kr)dk \qquad (9)
\end{aligned}$$

The shear source [$l = 1$ in Eq. (5)]:

$$\begin{aligned}
u_1 &= \frac{a\sigma_{13}(\omega)}{4\pi\mu}\int_0^\infty \left[-\frac{2k^2\nu'}{F(k)}e^{-\nu z} + \frac{(3k^2-k_\beta^2)(2k^2-k_\beta^2)-4\nu\nu'k^2}{\nu' F(k)}e^{-\nu' z}\right] J_1(ka)J_0(kr)dk \\
&+ \frac{a\sigma_{13}(\omega)cos2\phi}{4\pi\mu}\int_0^\infty \left[\frac{2k^2\nu'}{F(k)}e^{-\nu z} + \frac{(2k^2-k_\beta^2)-4\nu\nu'}{\nu' F(k)}k^2 e^{-\nu' z}\right] J_1(ka)J_2(kr)dk \\
u_2 &= \frac{a\sigma_{13}(\omega)sin2\phi}{4\pi\mu}\int_0^\infty \left[\frac{2k^2\nu'}{F(k)}e^{-\nu z} + \frac{(2k^2-k_\beta^2)-4\nu\nu'}{\nu' F(k)}k^2 e^{-\nu' z}\right] J_1(ka)J_2(kr)dk \\
u_3 &= \frac{a\sigma_{13}(\omega)cos\phi}{2\pi\mu}\int_0^\infty \left[-\frac{2\nu\nu'}{F(k)}e^{-\nu z} + \frac{2k^2-k_\beta^2}{F(k)}e^{-\nu' z}\right] J_1(ka)J_1(kr)kdk \qquad (10)
\end{aligned}$$

Eqs. (9) and (10) give elastic displacement at a field point anywhere in the half space for the compressional and shear sources. In practice, however, point measurements are not feasible and the wave signals are often measured using a receiver of finite size. In most cases, source and receiver are coaxially aligned, plane circular disks. It is a common practice to define the received signal as the average wave field over the receiver surface (Gitis and Khimunin, 1969; Tang et al., 1988). For a receiver transducer having the same radius as that of the source, the average field is given by:

$$\langle u_j\rangle = \frac{1}{\pi a^2}\int_0^{2\pi} d\phi \int_0^a u_j(r,\phi,z,\omega)rdr. \qquad (11)$$

By substitution of Eqs. (9) and (10) into Eq. (11), we obtain the averaged fields for the two sources:
The compressional source:

$$\begin{aligned}
\langle u_1\rangle &= 0 \\
\langle u_2\rangle &= 0 \\
\langle u_3\rangle &= -\frac{a\sigma_{33}(\omega)}{\pi\mu}\int_0^\infty \frac{2k^2-k_\beta^2}{F(k)}\nu e^{-\nu z}\frac{[J_1(ka)]^2}{ka}dk + \\
&+ \frac{2a\sigma_{33}(\omega)}{\pi\mu}\int_0^\infty \frac{k^2\nu}{F(k)}e^{-\nu' z}\frac{[J_1(ka)]^2}{ka}dk \qquad (12)
\end{aligned}$$

The shear source:

$$\begin{aligned}
\langle u_1 \rangle &= -\frac{a\sigma_{13}(\omega)}{\pi\mu}\int_0^\infty \frac{k^2\nu'}{F(k)}e^{-\nu z}\frac{[J_1(ka)]^2}{ka}dk + \\
&+ \frac{a\sigma_{13}(\omega)}{2\pi\mu}\int_0^\infty \frac{(3k^2-2k_\beta^2)(2k^2-k_\beta^2)-4\nu\nu'k^2}{\nu' F(k)}e^{-\nu' z}\frac{[J_1(ka)]^2}{ka}dk \qquad (13)\\
\langle u_2 \rangle &= 0\\
\langle u_3 \rangle &= 0
\end{aligned}$$

It is interesting to note that the average fields are polarized in the same direction as that of the source vibrations. A given shear or compressional source can generate both compressional and shear signals. The first integral in either Eq. (12) or Eq. (13) represents the compressional signal, while the second integral, the shear signal. However, as we will see in the next section, the wave amplitudes of shear waves produced by a compressional source and the compressional waves produced by a shear source are generally very small. Moreover, it will be instructive to compare Eqs. (12) and (13) with their acoustic counterpart (Williams, 1951). The average particle velocity potential $\langle\varphi\rangle$ is

$$\langle\varphi\rangle = 2av_0(\omega)\int_0^\infty \frac{exp(-\sqrt{k^2-k_c^2}z)}{\sqrt{k^2-k_c^2}}\frac{[J_1(ka)]^2}{ka}dk, \qquad (14)$$

where k_c is the acoustic wavenumber and $v_0(\omega)$ is the source particle velocity spectrum. Although the integrals in Eqs. (12) and (13) appear much more complicated than the one in Eq. (14), they have the common factors of the exponential function and the squared Bessel function. The similarity and difference between acoustic and elastic cases will be illustrated as we evaluate these integrals in the next section.

EVALUATION OF THE DIFFRACTION EFFECTS

To determine the diffraction effects due to the piston sources, we need to evaluate the integrals in Eqs. (12), (13), and (14). Although approximate solutions for the acoustic case (Eq. 14) were given by Williams (1951) and Bass (1958), it is difficult to obtain such closed form solutions for the integrals in Eqs. (12) and (13). In addition, approximate solutions are restricted by the assumptions under which they are valid. For example, Bass' (1958) expression is not applicable in the near field. We will use numerical methods to evaluate the integrals in Eqs. (12), (13), and (14). We transform the integrals into a form that is suitable for the Gauss-Laguerre algorithm of numerical integration.

The integrals in Eqs. (12), (13) and (14) are in the form of

$$I_\gamma = \int_0^\infty f(k) \frac{exp(-\sqrt{k^2 - k_\gamma^2}\, z)}{\sqrt{k^2 - k_\gamma^2}} \frac{[J_1(ka)]^2}{ka} dk, \tag{15}$$

where k_γ can be each one of k_α, k_β, and k_c, and $f(k)$ represents the remaining part of the integrand in these integrals (for example, $f(k) = 1$ in Eq. 14). We make the following change of variables:

$$\gamma = \sqrt{k^2 - k_\gamma^2}, \qquad Re\{\gamma\} \geq 0. \tag{16}$$

With this change of variables, the path of integration in the complex γ plane becomes path C in Figure 1. It should be noted that the integrand in Eq. (15) has singularities. For example, $k = k_\alpha, k = k_\beta, k = k_c$ are all branch points, and the term $1/F(k)$ contained in $f(k)$ (see Eqs. 12 and 13) has poles on the real k axis (Hanyga et al., 1985). All these singularities are mapped onto the real and imaginary axes of the γ plane (Figure 1). Therefore, integration along this path will have to consider the contributions from the singularities. To avoid this complexity, we make another change of variables,

$$\gamma = ik_\gamma + \gamma', \tag{17}$$

where γ' is a real variable. With this change of variables, we can deform path C into path C', which starts from $\gamma = ik_\gamma$ and goes to infinity parallel to the real γ axis (Figure 1). A careful study of the integrands of Eqs. (12), (13), and (14) indicates that they do not have singularities between path C' and the real γ axis. Thus the integration along path C is equivalent to the one along path C' according to the theorem of residues (an auxiliary path that links path C' with the real γ axis at infinity is ignored because of its zero contribution). Let

$$\gamma' = \bar{\gamma}/z, \tag{18}$$

and substituting into Eq. (15), we have

$$I_\gamma = e^{-ik_\gamma z} \frac{z}{a} \int_0^\infty \left\{ \bar{f}(\bar{\gamma}) \frac{\left[J_1(\frac{a}{z}\sqrt{\bar{\gamma}^2 + 2i\bar{\gamma}k_\gamma z})\right]^2}{\bar{\gamma}^2 + 2i\bar{\gamma}k_\gamma z} \right\} e^{-\bar{\gamma}} d\bar{\gamma}, \tag{19}$$

where $\bar{f}(\bar{\gamma})$ is $f(k)$ as the function of $\bar{\gamma}$, a dimensionless dummy variable. It is worthwhile to note that the propagation factor $e^{-ik_\gamma z}$ appears after the above transformations. Replacing k_γ by k_α, k_β, and k_c, we see that each integral in Eqs. (12), (13), and (14) corresponds to the signals that propagate with compressional, shear, and acoustic velocities, respectively. The diffraction effect comes from the integral in Eq. (19), which is to be evaluated. As clearly indicated in the equation, this integral is in the form of $\int_0^\infty g(x)e^{-x}dx$. This form of integration can be evaluated efficiently using the Gauss-Laguerre algorithm, although $g(x)$ is now a complex expression.

It should be pointed out that numerical problems may arise at high frequencies for large $k_\gamma z$. For large $k_\gamma z$, the Bessel function $J_1(\frac{a}{z}\sqrt{\bar{\gamma}^2 + 2ik_\gamma z\bar{\gamma}})$ approaches $J_1(\frac{a}{z}e^{i\pi/4}\sqrt{2k_\gamma z\bar{\gamma}})$, which blows up if the complex argument of the Bessel function is large. In practice this numerical problem often occurs at very high frequencies. This problem can be solved if we make use of the similarity between the elastic and acoustic diffractions at large $k_\gamma z$ values. Bass (1958) derived an approximate solution of Eq. (14) for the acoustic case. In terms of the integral in Eq. (15) for the acoustic case where $f(k) = \bar{f}(\bar{\gamma}) = 1$, this solution is given by

$$I_c(z, k_\gamma) \approx \frac{e^{-ik_\gamma z}}{ik_\gamma}\left\{1 - (1 - \frac{\xi^2}{2k_\gamma^2 a^2})[J_0(\xi) + iJ_1(\xi)]e^{-i\xi} - \frac{\xi^2}{k_\gamma^2 a^2}\left[\frac{iJ_1(\xi)}{\xi}\right]e^{-i\xi}\right\}, \quad (20)$$

where $\xi = \frac{k_\gamma}{2}(\sqrt{4a^2 + z^2} - z)$. For large $k_\gamma z$, this expression is very accurate (Gitis and Khimunin, 1969). For the elastic cases, the second integral in Eq. (12) and the first one in Eq. (13) approach zero as $k_\gamma z \to \infty$ (this will be demonstrated later), while the first integral in Eq. (12) and the second integral in Eq. (13) can be asymptotically evaluated by expanding $\bar{f}(\bar{\gamma})$ in series as $k_\gamma z \to \infty$.

$$\begin{aligned} \bar{f}(\bar{\gamma}) &\sim s^{-2} - \frac{i\bar{\gamma}}{k_\alpha z}(2s^{-2} - 4s^{-4} + 8s^{-5}) + \cdots, \quad (Eq.\ 12) \\ \bar{f}(\bar{\gamma}) &\sim 2 + \frac{i\bar{\gamma}}{k_\beta z}(2 - 8s^{-1}) + \cdots, \quad (Eq.\ 13) \end{aligned} \quad (21)$$

where $s = \alpha/\beta$. Substituting Eqs. (21) into Eq. (19) and taking only the leading order, we have the closed form asymptotic solutions for the elastic diffraction at large $k_\gamma z$. For the elastic case, the integrals represented by Eq. (15) become

$$\begin{aligned} I_\alpha &\sim s^{-2} I_c(z, k_\alpha), \quad k_\alpha z \to \infty, \\ I_\beta &\sim 2I_c(z, k_\beta), \quad k_\beta z \to \infty, \end{aligned} \quad (22)$$

where I_c is given by Eq. (20). By using the above numerical and asymptotic methods, we can evaluate the diffraction effects for different frequency range and receiver distances.

RESULTS

We first give an example of the evaluation of the average elastic fields. In this example, we let the compressional and shear velocities be $\alpha = 3.5\ km/s$ and $\beta = 2.2\ km/s$; we also let $\sigma_{13}(\omega) = \sigma_{33}(\omega) = \sigma_0 = const.$ (i.e., the source time function is a δ function). For a source transducer of radius $a = 10\ mm$ and a receiver of the same radius located at $z = 50\ mm$ away from the source, the results of the evaluations of Eqs. (12) and (13) in the frequency range of $0 - 1$ MHz are shown in Figure 2; the solid and dashed

curves in Figure 2a represent the compressional and shear wave spectra generated by a compressional piston source, while in Figure 2(b) the solid and dashed curves represent the shear and compressional spectra by a shear piston, respectively. As can be seen from these figures, the amplitudes of shear signals generated by a compressional source and the compressional signals by a shear source are very small. Also, one notices that the spectra of these signals are singular at zero frequency. Referring to the classical Lamb's problem (Pilant, 1979), we see that these signals are called "time integrals". This implies that in the frequency domain their spectra are divided by ω, which accounts for their singular behavior at zero frequency. Because the amplitudes of the time integrals are small, they can be ignored in practical applications, and we need only to consider the first term in Eq. (12) and the second term in Eq. (13).

Next we present the results of evaluation of the diffraction effects using both numerical and asymptotic methods in a broader frequency range ($0 - 2.5$ MHz). Using the same parameters as those used in Figure 2, we evaluate Eq. (15) for the compressional (the first integral in Eq. 12), shear (the second integral in Eq. 13), and acoustic (Eq. 14) cases. The results are shown in Figure 3. For comparison, the acoustic integral in Eq. (14) is multiplied by s^{-2} in Figure 3(a) and 2 in Figure 3(b), respectively (see Eq. 22). These integrals are calculated numerically using Eq. (19) in the lower frequency range, and asymptotically using Eqs. (20) and (22) in the higher frequency range. In both (a) and (b) of this figure, an arrow points to the frequency point at which the numerical and the asymptotic results are matched, and indeed the matches are excellent. For comparison we have also plotted the evaluation of the integral in Eq. (14) calculated entirely using Bass' formula (Eq. 20). The results are also multiplied by s^{-2} in Figure 3(a) and by 2 in Figure 3(b) for the comparison. We see that Bass' (1958) expression is significantly different from the numerically calculated result (dashed curves 1) near the zero frequency. This error has been pointed out by Tang et al. (1988). One notices from both (a) and (b) of this figure, that the dashed curves 1 that are based on the acoustic theory differ from the solid curves that are based on the elastic theory only at low frequencies. Our calculations show that this difference decreases with increasing receiver distances. A physical explanation is that, in the near field, the compressional or shear signal and its corresponding time integral are intimately coupled. As these signals propagate away from the source, they become decoupled because of their different propagation velocities and the rapid decay of the time integral with distance and frequency (Pilant, 1979). The higher the frequency, the faster the decoupling. This demonstrates that for large kz, the elastic diffraction of either a compressional or a shear wave approaches acoustic diffraction, as appears on Figure 3. This is to be expected since in the far field, both the compressional and shear waves obey their own scalar wave equations in an isotropic homogeneous medium. One recalls Kirchhoff's pioneer work on the diffraction of light by a circular aperture. Although Kirchhoff used the scalar diffraction theory to explain the behavior of a vector field, the later vector approach of Smythe did not change his conclusion in the axial region of the Fraunhofer zone (see Jackson, 1962). This historic example,

together with the present example, reveals the governing principles residing in classical continuum physics, be they electromagnetic or elastodynamic.

APPLICATION

An important application of the study of diffraction effects is in wave attenuation measurements. As we have seen in Figures 2 and 3, diffraction effects result in the decay of wave amplitude with increasing frequency, even in the absence of intrinsic damping. Consequently, in attenuation measurements using the amplitude decay of wave trains, the intrinsic attenuation will be overestimated, while in the attenuation measurements using spectral ratio methods (Toksöz et al., 1978; Tang et al., 1988), the diffraction effects can cause the intrinsic attenuation to be either over or underestimated, depending on whether samples of different lengths or of different acoustic properties are used. To illustrate this effect, let us consider the case of a wave signal generated by a cylindrical source, propagated through a sample, and recorded by a receiver. Then the received wave spectrum is given by

$$A(\omega) = \sigma(\omega)e^{-ikz}G(\omega; a, z, \alpha, \beta)R(\omega), \tag{23}$$

where $\sigma(\omega)$ is the source stress spectrum of either a compressional or shear source, a is the transducer radius, $R(\omega)$ is the instrument transfer function of the recording system, G is the geometric spreading factor. $e^{-ikz}G$ is equivalent to I_γ in Eq. (19), where I_γ can be either I_α or I_β depending on whether a shear or compressional signal is measured. The propagation factor e^{-ikz} contains the intrinsic attenuation when the wavenumber k is made complex,

$$k = \omega/v - i\eta, \tag{24}$$

where v is shear or compressional velocity and η is the attenuation coefficient given by

$$\eta = \frac{\omega}{2Qv}, \tag{25}$$

where Q is the quality factor of the sample. Suppose that measurements are made with two samples using the same source and receiver. By taking the ratio of the amplitude spectra of the two received signals and using Eqs. (23) and (24), we obtain

$$\eta_1 z_1 - \eta_2 z_2 = ln\frac{|A_2(\omega)|}{|A_1(\omega)|} + ln\frac{|G_1(\omega; a, z_1, \alpha_1, \beta_1)|}{|G_2(\omega; a, z_2, \alpha_2, \beta_2)|}, \tag{26}$$

where subscripts 1 and 2 refer to measurements 1 and 2 and ln denotes the natural logarithm. Two methods can be used to determine attenuation using Eq. (26). The first is to use two samples of the same material with different lengths. The second is to use a reference sample (say sample 1) with known Q, α, and β values and

determine the attenuation of the sample of interest relative to the reference sample. The reference sample is chosen to be a non-attenuating material, such as aluminum, whose $Q \approx 150,000$ (Zemanek and Rudnick, 1961). In both cases, the attenuation of the second sample η_2 (or $1/Q_2$) can be determined from the measured spectral ratio $|A_2(\omega)|/|A_1(\omega)|$ provided that the geometric spreading term $ln(|G_1|/|G_2|)$ as a function of frequency is known (Eq. 19).

To test the elastic diffraction theory developed in this study, we carried out laboratory experiments using compressional wave sources and aluminum and lucite as samples. Table 1 shows the properties of these materials. The samples are cylinders with a radius of 76 mm and different lengths ranging from 24 mm to 64 mm. The source and receiver transducers were mounted at the opposite ends. The transducers were piezoelectric transducers, Panametrics $V303$ and $V152$, circular in shape. The former has a radius of 7 mm, and the latter 14 mm. The center frequency is around 1 MHz. Figure 4 shows the experimental set up.

To study the effects of diffraction on the measurement of attenuation using samples of the same material with different lengths, we measure aluminum samples of lengths 24 mm and 64 mm. Since aluminum has very low attenuation (Zemanek and Rudnick, 1961), these measurements are ideal to determine the effects of diffraction. Figure 5(a) shows the amplitude spectra of transmitted waves for 24 mm and 64 mm long samples. The transducers are the same in both cases, with radius $a = 7$ mm. The different amplitudes are due to diffraction (or spreading) effects. The $ln(|A_2|/|A_1|)$ curve calculated from the spectra in Figure 5(a) is shown in Figure 5(b) (dashed curve). This curve has a positive slope. However, the (very small) intrinsic attenuation should cause the $ln(|A_2|/|A_1|)$ curve to have a slight negative slope when plotted versus frequency. Consequently, the observed effect is due to diffraction. The diffraction (or beam spreading) effect can be corrected by the term $ln(|G_1|/|G_2|)$ in Eq. (26) using the expression given in Eq. (19). When the correction is made, the $ln(|A_2|/|A_1|)$ curve is returned almost to the zero line, as shown in Figure (5)b (solid curve). Since the aluminum has almost no intrinsic attenuation, the log amplitude ratio curve should be almost flat, thus theory and experiment agree very well in this case.

To study the effects of transducer radius, we repeated the above experiment using transducers of radius $a = 14$ mm. Figure 6(a) shows the measured wave spectra. As compared to Figure 5(a), the larger transducers produce smaller diffraction effects. However, the measured $ln(|A_2|/|A_1|)$ curve in Figure 6(b) still shows a non-negligible positive slope (dashed curve). After correction, the $ln(|A_2|/|A_1|)$ curve is returned to the zero line. There are some fluctuations about the zero line (solid curve). These fluctuations probably imply that for large transducers, the assumed constant stress distribution over the source surface and the constant weight average operation, as used in our theory (Eqs. 6 and 11), may be oversimplified in the near field. (Note that the sample is only 24 mm long, which is less than the diameter (28 mm) of the

transducer.)

Next we study the effects of diffraction in the measurement of attenuation using a reference sample. This technique is used extensively for laboratory measurements (Toksöz et al., 1978). aluminum is chosen to be the reference, while lucite is the measurement sample. We first use the $a = 7\ mm$ transducers. Figure 7(a) shows the measured wave spectra for the $64mm$ long aluminum reference and the $38mm$ long lucite sample. Figure 7(b) gives the $ln(|A_2|/|A_1|)$ curve (dashed curve) calculated using the spectra in Figure 7(a). Then the correction term $ln(|G_1|/|G_2|)$ is calculated using Eq. (19) and used to obtain the corrected curve (solid curve). As seen from this figure, the correction is significant, because the shear and compressional velocities of the aluminum are much higher than those of the lucite (see Table 1). The curves in Figure 7(b) can be linearly fitted versus frequency to give the quality factor Q of the material (Toksöz et al., 1978). Due to the great influence of the diffraction effects in this particular case, the uncorrected curve gives a Q_α value of 30, whereas the corrected curve gives a Q_α of 72. We repeated the lucite-aluminum experiment using larger ($a = 14\ mm$) transducers. Figure 8(a) shows the measured wave spectra for the 51 mm long aluminum the 38 mm long lucite damples. The uncorrected and corrected attenuation curves are shown in Figure 8(b). The linear trend of the corrected curve becomes apparent. The linear part of this curve gives a Q_α value of 76 for lucite, agreeing with the previous estimate of Q_α of 72, and the uncorrected curve gives a Q_α value of 50.

The above experiments demonstrate that the effects of diffraction are maximized when small transducers, short samples, and samples of very different acoustic properties are used. In the attenuation measurements commonly executed in rock physics, the diffraction effects can be minimized by using larger transducers, and by choosing a reference sample whose acoustic properties are close to those of the measurement samples, such that the correction term $ln(|G_1|/|G_2|)$ can be regarded as independent of frequency in the frequency range of measurement. In cases where the diffraction effects are not negligible, the diffraction theory developed in this study can be used to make the correction. Finally, when large transducers are used such that the received waves are sensitive to the details of stress distribution over the source surface, Eq. (5) can be used to calculate the wave radiation and diffraction provided that this distribution can be obtained.

CONCLUSIONS

In this study, we investigated the radiation and diffraction of the elastic wave field generated by a piston (cylindrical) source. Using the elastic representation theorem and the corresponding tensor Green's function, we presented a formulation that can be used to calculate the radiated elastic wave field for any given piston shape and source

stress distribution. Assuming a constant compressional or shear stress distribution over a circular piston surface, we derived the integral expressions for the radiated elastic wave field. On the basis of these expressions, we obtained the average wave field received by a receiver coaxially aligned with the source. Despite the complexity of elastic radiation, the average field was found to polarize in the source stress direction. For evaluating the diffraction effects, we used numerical techniques in the near field and asymptotic techniques in the far field. It was shown that a compressional or a shear piston generates a mainly compressional or shear signal in the axial direction, together with some time integral signals which decay rapidly in the far field. Thus in the far field, the radiation and diffraction of either a compressional or a shear wave are very similar to those of an acoustic wave, despite the vector nature of the elastic waves. In particular, we studied the effects of elastic diffraction in conjunction with elastic attenuation measurements. The experimental results were found to agree well with the theory, and the correction for the diffraction effects gave a reasonable estimate of the attenuation for the material measured. Although we only did measurements with compressional waves, the shear waves can be treated in much the same way. The knowledge obtained from this study will be useful in scientific applications where piston sources are used.

ACKNOWLEDGEMENTS

We would like to thank Tien-When Lo for his helpful discussions and help in the experimental set up. Karl Coyner of New England Research Inc. provided the samples for the experiment. This research was supported by AFGL contract No. F19628-86-K-0004, DOE grant No. DE-FG02-86ER13636, and by the Full Waveform Acoustic Logging Consortium at M.I.T.

REFERENCES

Aki, K., and Richards, P., *Quantitative Seismology–Theory and Methods,* W.H. Freeman and Co., San Francisco, 1980.

Bass, R., Diffraction effects in the ultrasonic field of a piston source, *J. Acoust. Soc. Am., 30,* 602–605, 1958.

Gitis, M.B., and Khimunin, A.S., Diffraction effects in ultrasonic measurements, *Sov. Phys. Acoust., 14,* 413–431, 1969.

Hanyga, A., Lenartowicz, E., and Pajchel, J., *Seismic Propagation in the Earth,* Elsevier, 1985.

Harris, G.R., Review of transient field theory for a baffled planar piston; *J. Acoust. Soc. Am., 70,* 10–20, 1981.

Jackson, J.D., *Classical Electrodynamics,* John Wiley & Sons, Inc., New York, 1962.

Johnson, L.E., Green's function for Lamb's problem, *Geophys. J. Roy. Astr. Soc., 37,* 99–131, 1974.

Pilant, W.L., *Elastic Waves in the Earth,* Elsevier, 1979.

Tang, X.M., Toksöz, M.N., Tarif, P., and Wilkens, R.H., A method for measuring acoustic wave attenuation in the laboratory, *J. Acoust. Soc. Am., 83,* 453–462, 1988.

Toksöz, M.N., Johnston, D.H., and Timur, A., Attenuation of seismic waves in dry and saturated rocks: I. Laboratory measurements, *Geophysics, 44,* 681–690, 1978.

Williams, A.O., Jr., The piston source at high frequencies, *J. Acoust. Soc. Am.,* 23, 1–6, 1951.

Zemanek, J., and Rudnick, I., Attenuation and dispersion of elastic waves in a cylindrical bar, *J. Acoust. Soc. Am., 33,* 1283–1288, 1961.

Sample	ρ (g/cm^3)	α (m/sec)	β (m/sec)
Aluminum	2.7	6410	3180
Lucite	1.2	2740	1330

Table I: Density ρ, compressional velocity α, and shear velocity β of the samples used in the measurement.

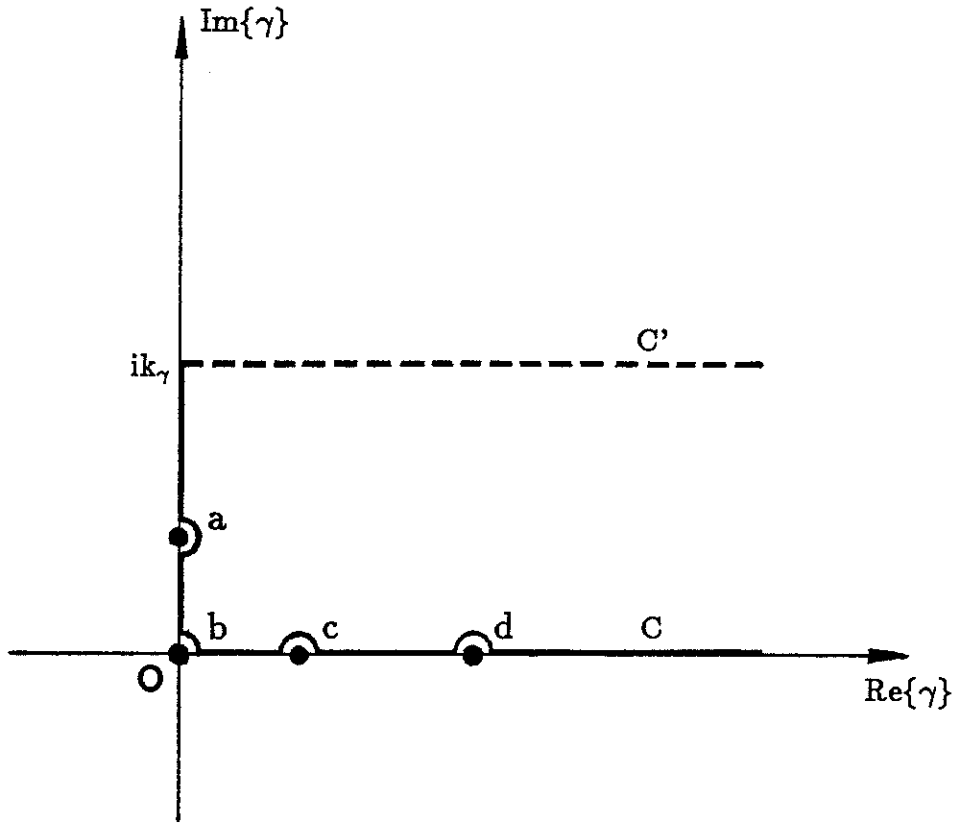

Figure 1: Paths of integration in the complex γ plane. Path C which passes through singularities is deformed into path C' to facilitate the numerical evaluation. The small solid circles represent singularities. For $k_\gamma = k_c$, Eq. (15) has only one singularity (b) at $\gamma = 0$. For $k_\gamma = k_\alpha$ and $k_\gamma = k_\beta$, Eq. (15) correspond to the integrals in Eqs. (12) and (13). The singularities are $\gamma =$ (a) $i\sqrt{k_\beta^2 - k_\alpha^2}$, (b) 0, (c) $\sqrt{k_\beta^2 - k_\alpha^2}$, and the one furthest to the right of the real γ axis, (d), which is a zero of $F(k)$ in Eqs. (12) and (13).

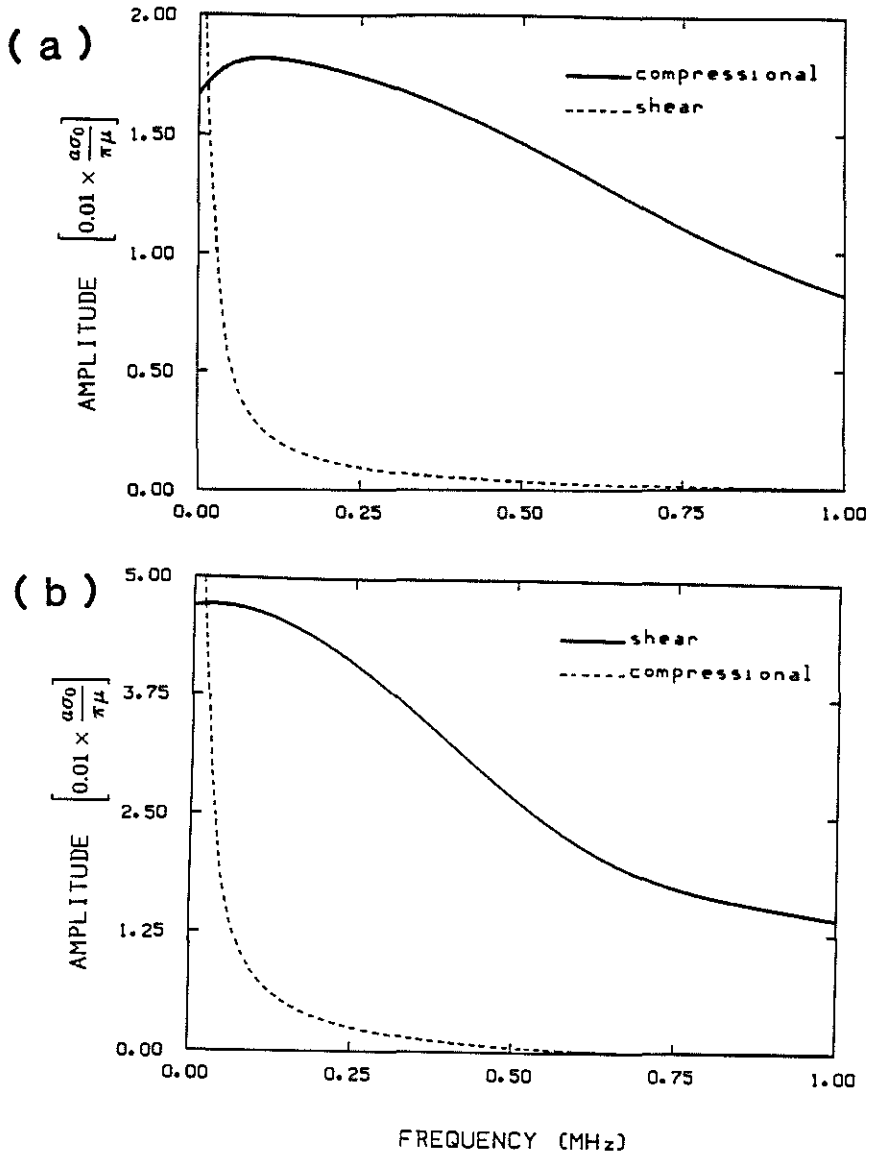

Figure 2: Numerical evaluations of Eqs. (12) and (13) for $\alpha = 3.5\ km/sec$, $\beta = 2.2\ km/sec$, $z = 50\ mm$, and $a = 10\ mm$. (a) Eq. (12), for the compressional source. (b) Eq. (13), for the shear source. In (a), the solid and dashed curves are the compressional and shear wave amplitude spectra generated by the compressional source, while in (b), the solid and dashed curves are the shear and compressional spectra generated by the shear source. The dashed curves correspond to the time integrals, which decay rapidly with increasing frequency.

Figure 3: Evaluation of Eq. (15) for the compressional, shear, and acoustic cases using numerical and asymptotic methods. The parameters used are the same as those in Figure 2. (a) Compressional (solid curve) versus acoustic (dashed curve 1), where the acoustic velocity equals the compressional velocity. (b) shear (solid curve) versus acoustic (dashed curve 1), where the acoustic velocity equals the shear velocity. In both (a) and (b), the solid curves and the dashed curves 1 are calculated numerically in the lower frequency range, and asymptotically in the higher frequency range. The arrows point to the frequency at which the results of both methods are matched. The dashed curves 2 correspond to the acoustic integrals [$k_c = k_\alpha$ in (a) and $k_c = k_\beta$ in (b)] asymptotically evaluated using Bass' expression (Eq. 20). Note that the dashed curves 1 and 2 are significantly different at low frequencies. The acoustic curves have been multiplied by a factor of β^2/α^2 in (a) and of 2 in (b) for the comparison (see Eqs. 22).

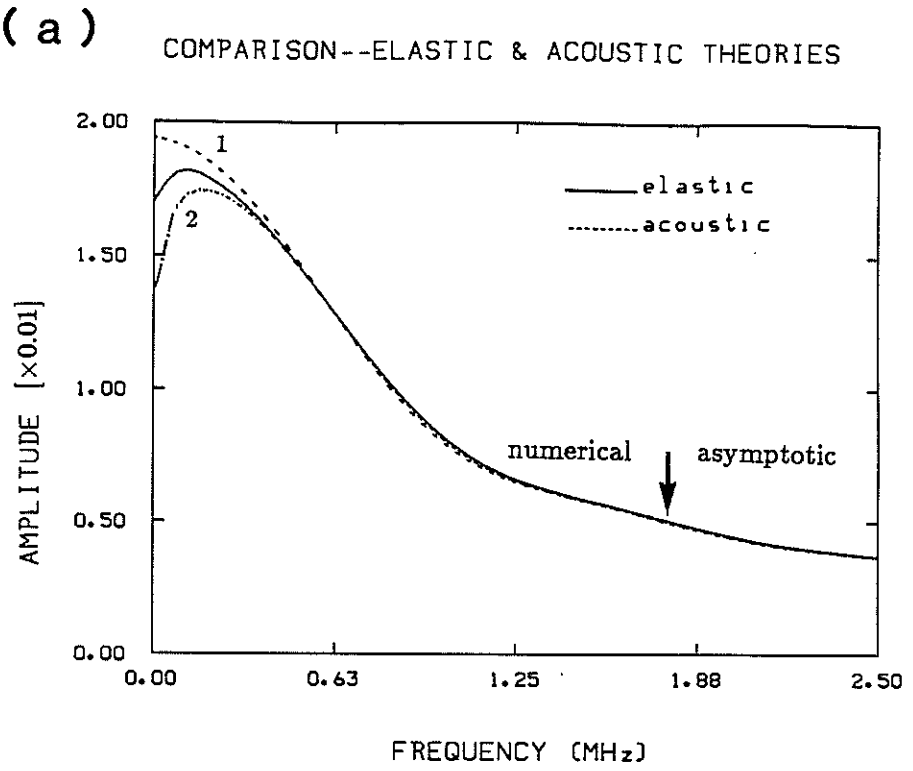
(a)
COMPARISON--ELASTIC & ACOUSTIC THEORIES
2.00
1.50
1.00
0.50
0.00
AMPLITUDE [×0.01]
1
2
elastic
acoustic
numerical
asymptotic
0.00
0.63
1.25
1.88
2.50
FREQUENCY (MHz)

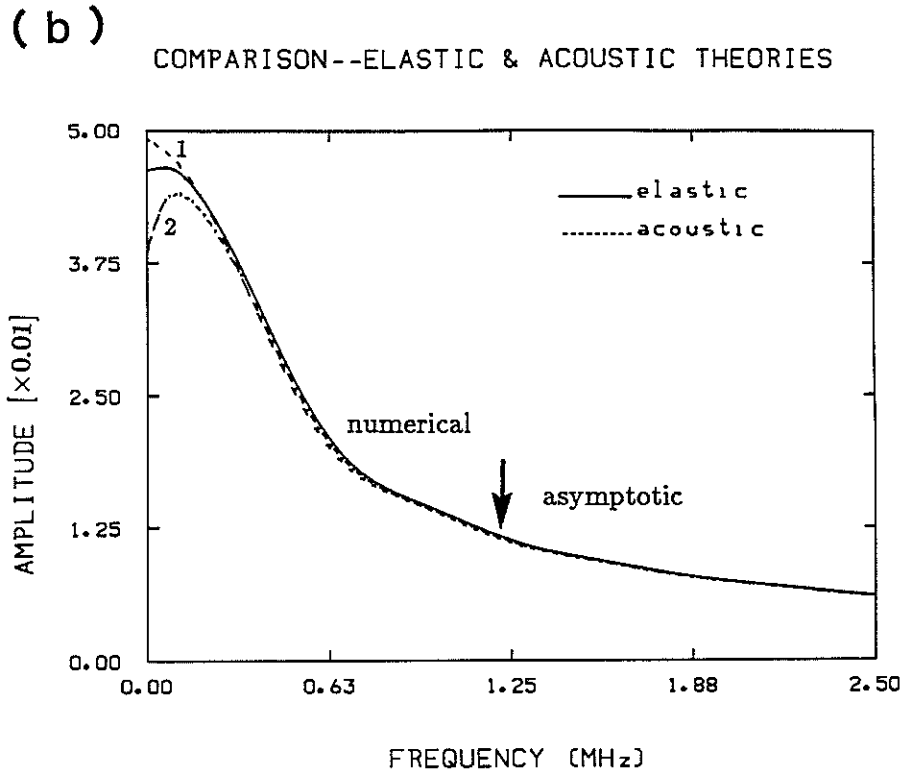
(b)
COMPARISON--ELASTIC & ACOUSTIC THEORIES
5.00
3.75
2.50
1.25
0.00
AMPLITUDE [×0.01]
1
2
elastic
acoustic
numerical
asymptotic
0.00
0.63
1.25
1.88
2.50
FREQUENCY (MHz)

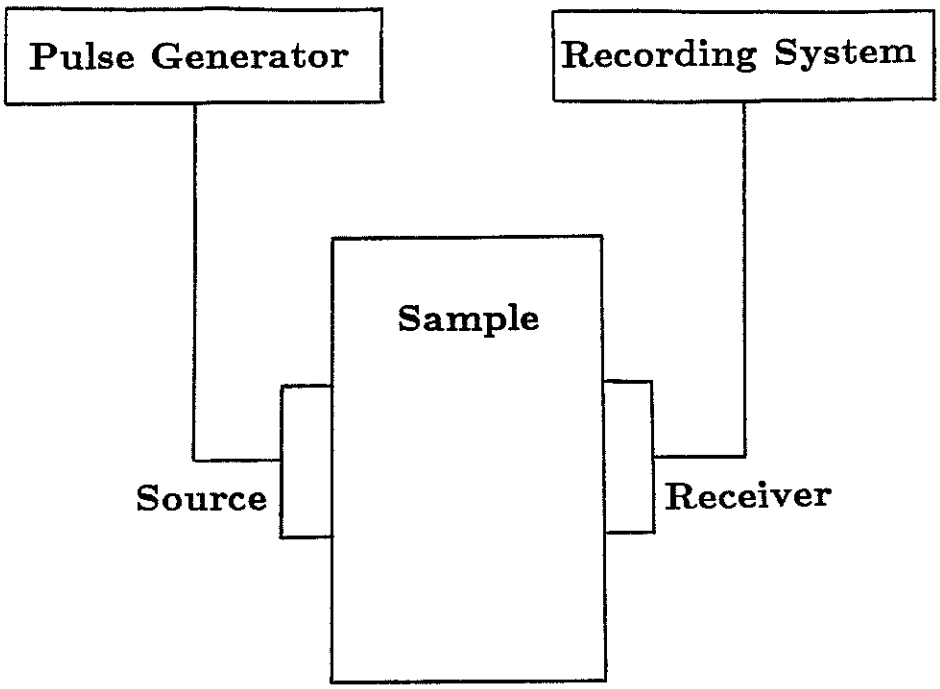

Figure 4: Experimental set up. The source and the receiver are mounted at the opposite ends of the sample. The source transducer generates a wave signal, which propagates through the sample, and is recorded by the receiving system.

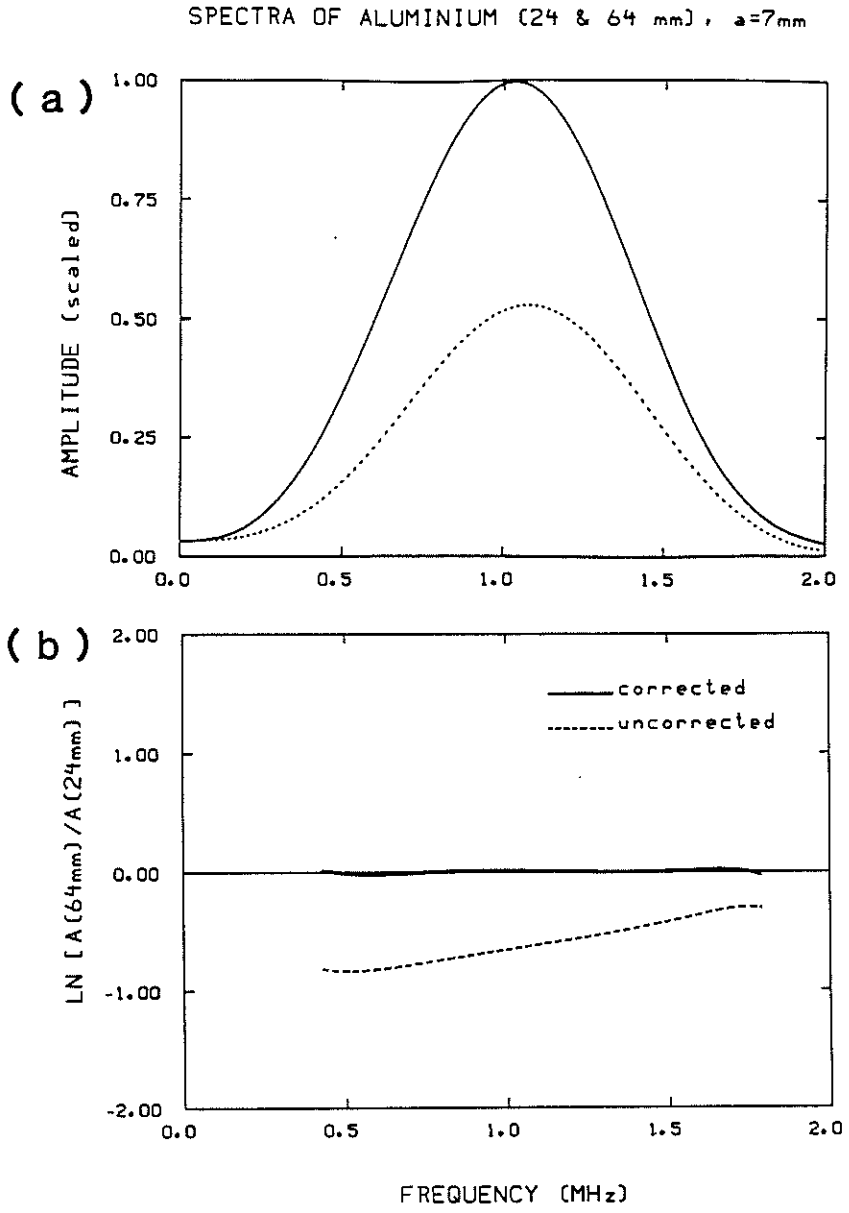

Figure 5: (a) Amplitude spectra of compressional waves generated and received by transducers with $a = 7\ mm$ radii. The source and the receiver are coaxially aligned, as shown in Figure 4. The medium of propagation is aluminum. Sample lengths are 24 mm (solid curve) and 64 mm (dashed curve). (b) The measured spectral ratio $ln(|A_2|/|A_1|)$ (dashed curve) and its correction (solid curve) for the diffraction effects. Note that the uncorrected curve has a positive slope and that the corrected curve coincides with the zero line.

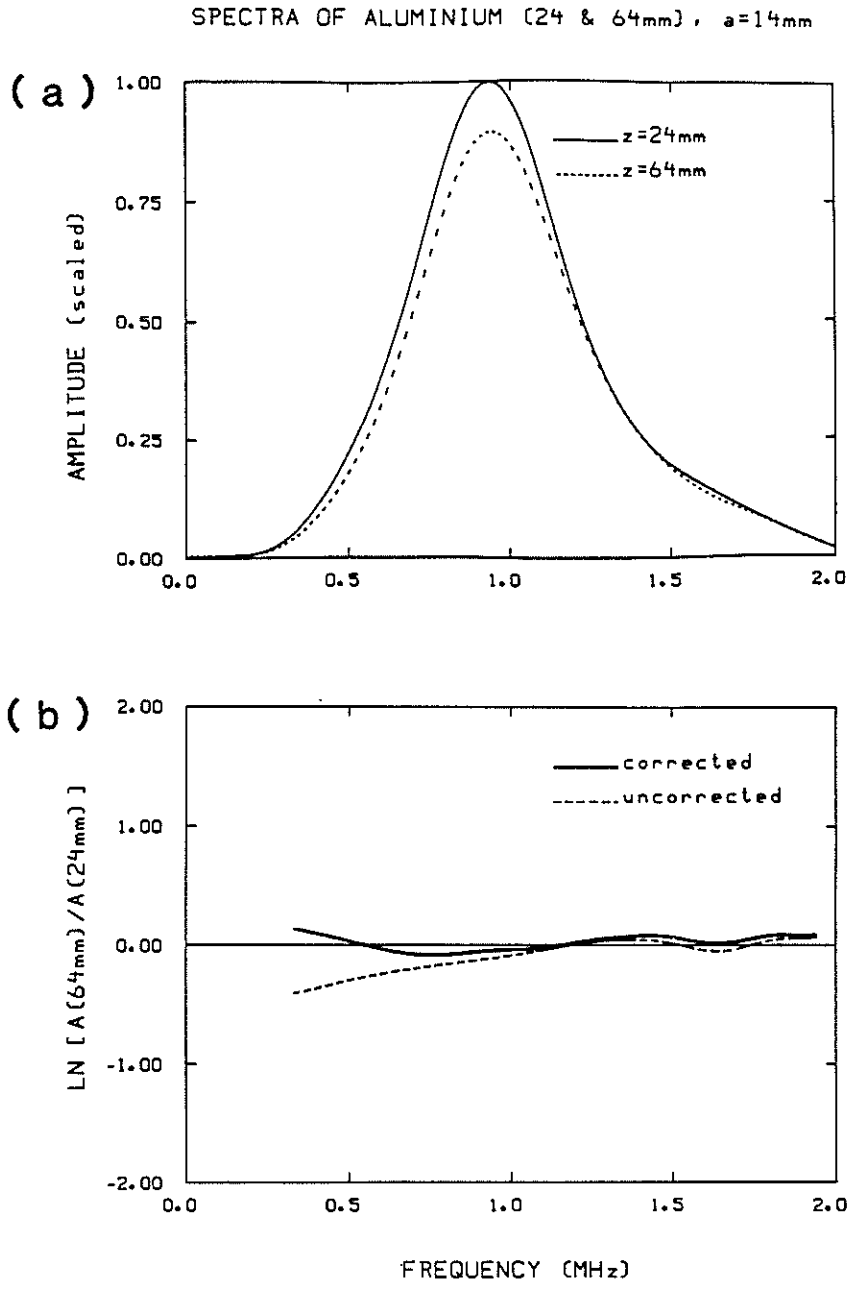

Figure 6: Same as Figure 5, but now the transducers have $a = 14\ mm$ radii.

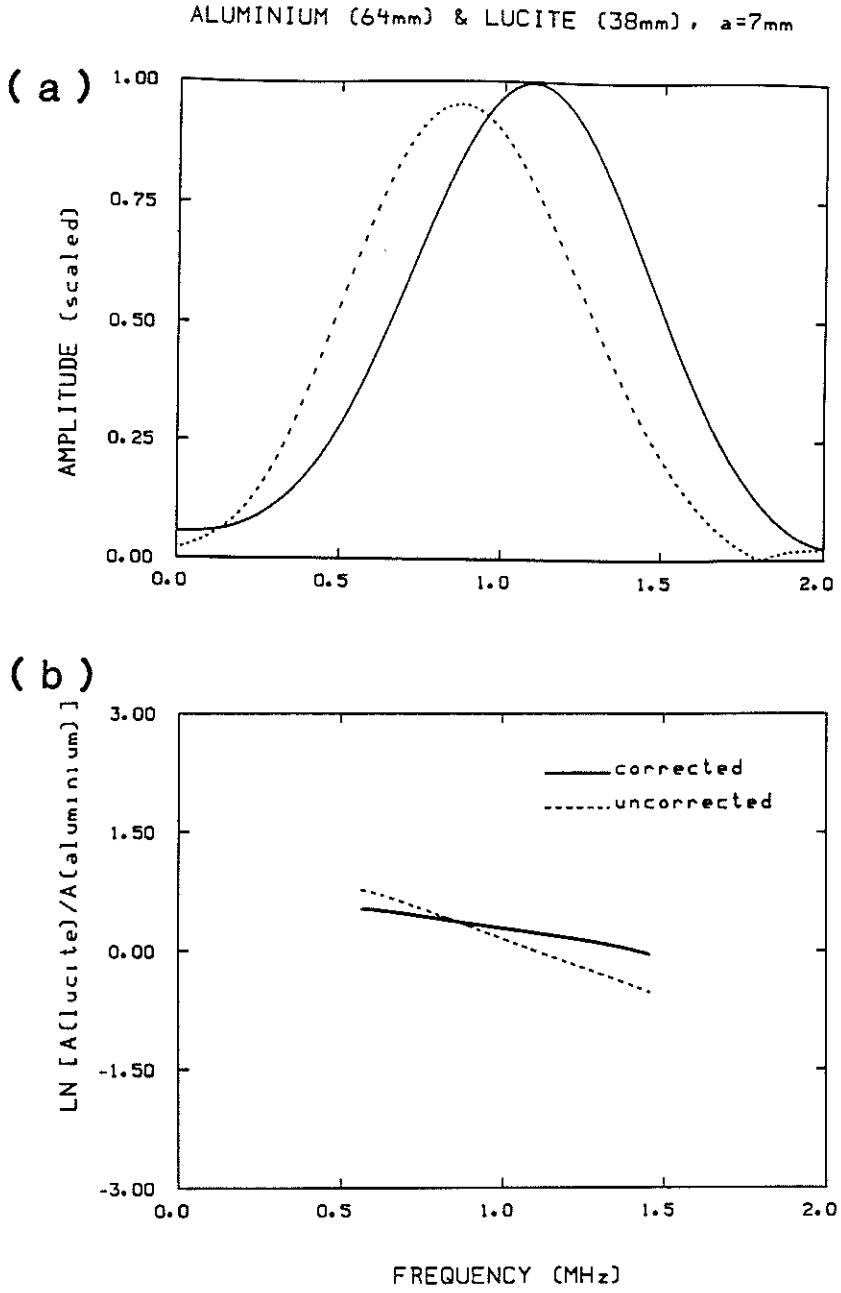

Figure 7: (a) Wave spectra of aluminum ($z = 64\ mm$) (solid curve) and lucite ($z = 38\ mm$) (dashed curve). (b) The measured spectral ratio (dashed curve) and its correction (solid curve) for the diffraction effects. Note that the slope of the corrected curve is decreased.

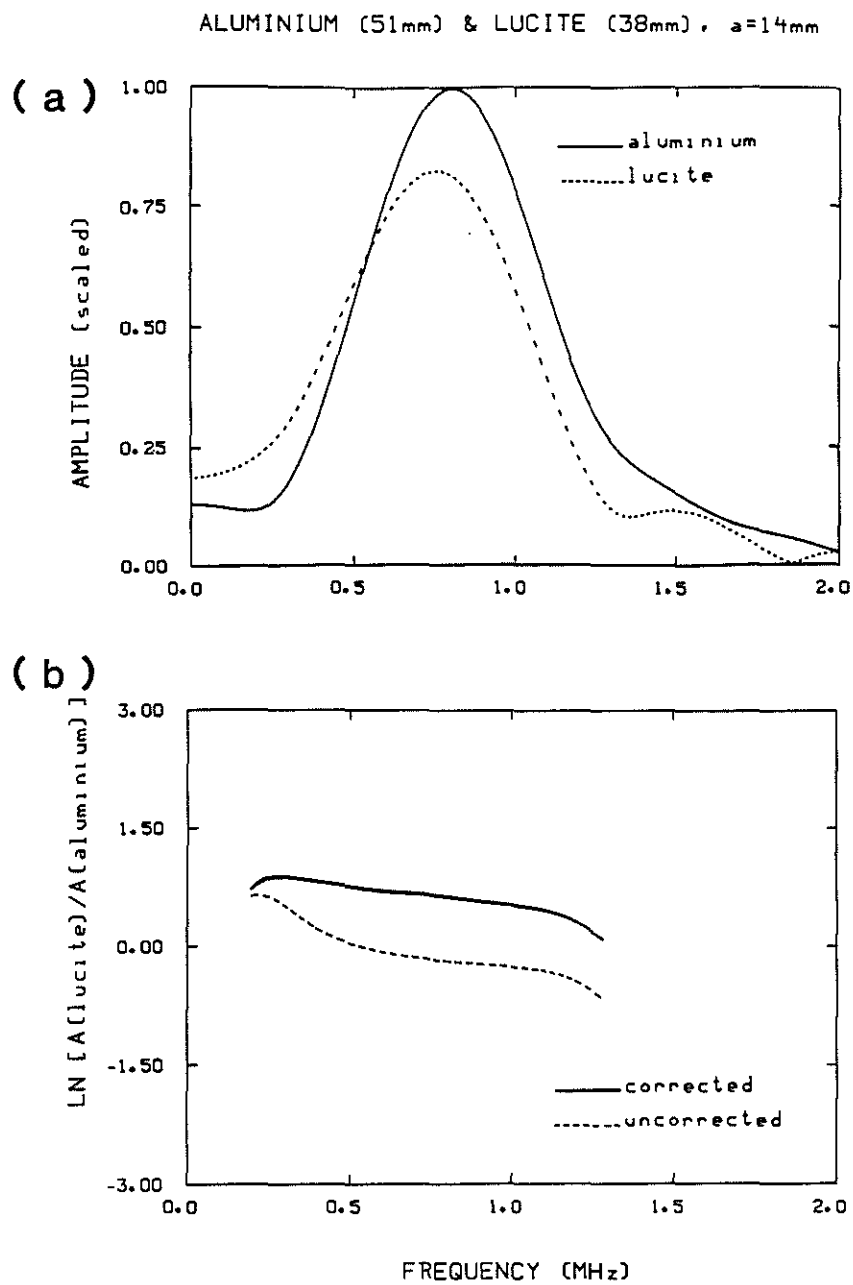

Figure 8: (a) Wave spectra of aluminum ($z = 51\ mm$) (solid curve) and lucite ($z = 38\ mm$) (dashed curve). (b) The measured spectral ratio (dashed curve) and its correction for the diffraction effects. Note that the linear trend of the corrected curve becomes apparent.